J Mater Sci (2011) 46:1916–1931
DOI 10.1007/s10853-010-5027-x

Polymer matrix–clay interaction mediated mechanism of electrical transport in exfoliated and intercalated polymer nanocomposites

A. L. Sharma · Awalendra K. Thakur

Received: 19 July 2010 / Accepted: 21 October 2010 / Published online: 3 November 2010

Abstract We report significant results on charge transport phenomena in the exfoliated and intercalated phase of polymer nanocomposite (PNC). X-ray diffraction and transmission electron microscopy results have provided convincing evidence of exfoliation at lower clay loading ($x < 5$ wt%) and intercalation at higher clay loading ($x > 5$ wt%) in the PNC. Fourier transform infrared (FTIR) spectrum indicated lowering of anion symmetry from O_h to $C_{4v}/C_{2v}/C_{3v}$ (depending on mode of cation interaction with counter ion). Substantial jump in electrical conductivity ($\sim$110 times) at room temperature has occurred on nanocomposite formation in sharp contrast to that of the polymer salt (PS) complex film. Large conductivity enhancement (10^{-3} S cm^{-1}) is attributed to clay-induced interaction with PS matrix whose origin lies in polymer–ion, ion–ion, ion–clay, and polymer–ion–clay interaction evidenced in the FTIR results. An excellent correlation of conductivity with fraction of free anion and polymer glass-transition temperature agrees well with conductivity enhancement at specific clay loading. A model for charge transport phenomena is proposed to explain clay-induced ion dynamics. The conceptual basis of the model seems consistent with experimental results.

A. L. Sharma · A. K. Thakur (✉)
Department of Physics and Meteorology,
Indian Institute of Technology (IIT), Kharagpur 721302, India
e-mail: akt@phy.iitkgp.ernet.in

A. K. Thakur
Department of Physics, Indian Institute of Technology (IIT),
Patna, India
e-mail: akt@iitp.ac.in

Introduction

Ionically conducting solid polymer films have been utilized in many energy related sectors like high energy density solid polymer batteries, PEM fuel cells, and supercapacitors, etc. [1–4]. Such applications require a desirable conductivity value $\sim 10^{-3}$ S cm^{-1} at room temperature. In order to achieve this conductivity value, a large variety of ion-conducting material systems such as solid polymer electrolytes (SPEs) [5–7], gel polymer electrolytes (GPEs) [8, 9], and composite polymer electrolytes (CPEs) [9, 10], etc. have been prepared and evaluated. However, most of the systems have exhibited conductivity much lower than the desirable value for device application under ambient conditions. However, a number of limitations came to be identified later, when evaluated for their suitability in device application. The basic factor imposing severe restraint on their applicability are (i) low ambient ionic conduction, (ii) concentration polarization, and (iii) poor stability (thermal, mechanical, chemical and electrochemical, etc.) properties. Another reason for lower ionic conduction is concentration polarization whose origin lies in ion association (ion pairing) effect [11, 12] due to the presence of both cations and anions in the host polymer matrix. As a consequence, internal resistance of the polymer film builds up, this in turn, reduces ion (charge) transport whenever excess number of ion pairs are there in the host polymer matrix in comparison to the available number (fraction) of free charge carrier (i.e., anion and hence cation). Strong coulombic interaction among oppositely charged ions in the host polymer matrix is solely responsible for ion pairing effect and concentration polarization. The reasons identified for poor ambient conduction are slow ion dynamics in a multiphase polymeric matrix and poor segmental (chain) mobility in polymers at room

temperature in addition to the usual causes such as ion–ion interaction (pairing effect). In the case of gel polymer electrolyte (GPEs), conductivity has been observed to be $\sim 10^{-3}$ S cm^{-1} in a number of cases. [13–16] But, they have inherent problems of poor mechanical and thermal stabilities, presence of solvent in the matrix imparting semi-solid/semi-liquid behavior that causes specific problems of chemical stability/reactivity at the electrolyte–electrode interface on device fabrication.

In order to overcome/improve upon the limitations mentioned above, several approaches have been suggested, tried, and evaluated. A recent innovative approach of nanocomposite formation via intercalation of cation coordinated polymer chains into nanometric clay channels of an organophilic clay (such as dodecylamine (DDA)-modified montmorillonite clay or DMMT) having a compatible gallery width just enough to accommodate cations ($Li^+ \sim 0.76$ Å) restricting the entry of bulky anions ($\sim$2.8 Å) has opened a new direction with numerous possibilities. Conceptually, it appears that this approach may minimize concentration polarization arising due to coulombic interaction between cations and anions (i.e., ion association effect) at a desirable level. A quantitative estimation of the concentration polarization, expressed in terms of the fraction of free anions/cations and ion pairs present in the composite matrix, has provided sufficient and valuable insight into the actual role of ion association (pairing) and dissociation effects on electrical conduction property of the intercalated polymer nanocomposite (PNC) films. The presence of a third component such as an organic/inorganic clay in a heterogeneous polymer composite film also affects the polymer–ion and ion–ion interactions via direct interaction of the filler component with the cation coordinated polymer matrix [where the cation coordinated to the electron-rich group in the host polymer matrix, e.g., –Ö– in polyethylene oxide (PEO), –C≡N̈ in polyacrylonitrile (PAN), etc.]. The strength of such an interaction depends on the filler properties (i.e., chemical nature, electrical properties such as the presence of dipoles) and its concentration in the composite matrix.

In this article, we report a series of lithium ion conducting polymer nanocomposite (PNC) film comprising an amorphous polymer host (polyacrylonitrile PAN), a lithium salt ($LiPF_6$), and organophilic clay (DMMT). The organomodified clay have enhanced nanometric clay channel width (6 Å) with high cation exchange capacity (CEC) $\sim$ 80–120 mEq/100 g [17] and the presence of negative charges on the surface of clay layers after organomodification. As a consequence it may be expected to favor a preferential entry of the cation coordinated polymer matrix into the clay channels and impose a practical limitation on anions coming into the close proximity of the cations [18]. So, the possibility of ion pair formation caused by attractive columbic forces may be expected to be minimum. Such feasibility has been studied and correlated with clay concentration dependence on electrical conductivity. The interaction among the composite components has been investigated systematically using Fourier transform infrared (FTIR) spectroscopy. The experimental results provide evidence of polymer–ion–clay interaction that enabled us to propose a model to understand the ion dynamics and charge transport process in intercalated/exfoliated polymer nanocomposite films.

Experimental

Materials preparation

Polymer nanocomposite (PNC) films were prepared via a standard solution cast technique. The polymer salt (PS) complexation was performed using polyacrylonitrile (PAN; Aldrich M.W. 1.5×10^5) as the polymer host matrix, and appropriate stoichiometry of lithium salt ($LiPF_6$; Aldrich) having bulky anion (PF_6^-). The polymer host (PAN) and salt ($LiPF_6$) was vacuum-dried at 120 °C for 32 h prior to sample preparation. An appropriate stoichiometric ratio of PAN was dissolved in *N*,*N*-dimethylformamide (DMF; Merck) and the solution was stirred for 18 h. Subsequently, a calculated amount of $LiPF_6$, was added into the PAN solution and stirred for 15 h to facilitate homogeneous mixing and complexation. The stoichiometric ratio of salt in the polymer host (PAN) matrix was maintained at an optimized ratio of ($\ddot{N}/Li = 8$). Nanocomposite formation was carried out via intercalation of cation coordinated polymer chains (PS) into nanometric clay channels of the DDA-modified montmorillonite clay (DMMT). Next, clay modification was carried out with DDA modifier as per the following flow chart as shown in Fig. 1. DDA-modified montmorillonite clay was added into the complex polymer salt solution in different concentrations ($0 \leq x \leq 20$; x refers to clay concentration w.r.t. PAN by wt.) and stirred for 12 h. Finally, the composite solutions were poured in polypropylene dishes and allowed to dry under controlled conditions. Free-standing polymer nanocomposite films were obtained on solvent evaporation. The series of polymer nanocomposite (PNC) films so obtained can be expressed as: $(PAN)_8LiPF_6 + x$wt% DMMT.

Material characterization

The X-ray diffraction (XRD) data have been collected at room temperature by a 'X'Pert PRO PANalytical

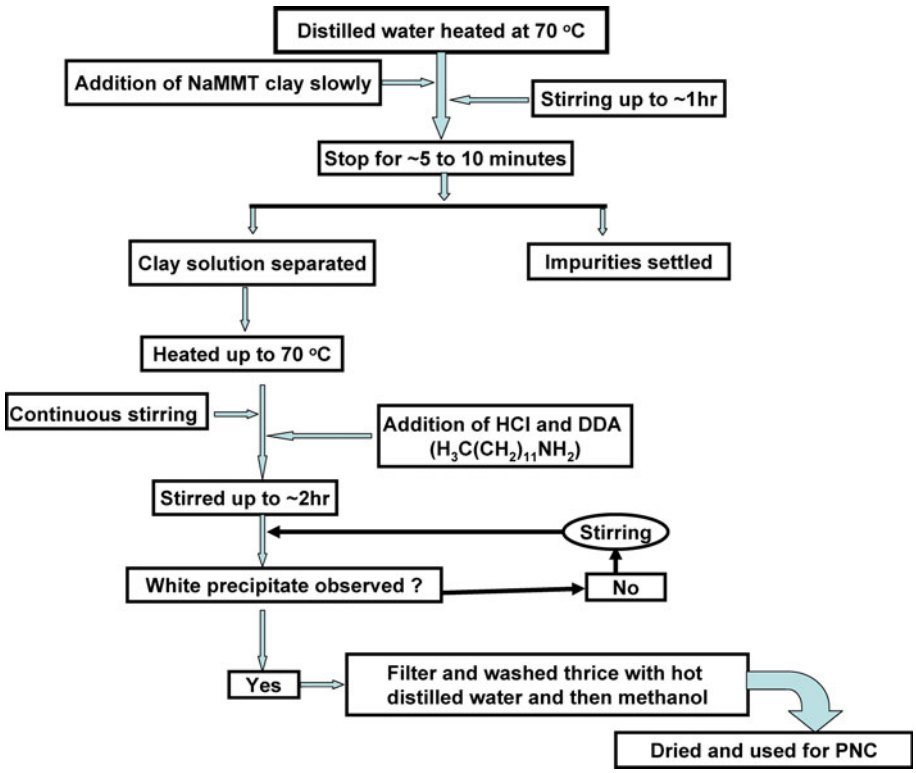

Fig. 1 Flowchart diagram of clay modification

diffractometer (model: PW3040/60) with CuKα radiation ($\lambda = 1.5418$ Å) over a range of diffraction angle ($2° \leq 2\theta \leq 40°$) at a scanning rate of 2°/min. Transmission electron microscopy (TEM) has been performed by JEOL-JEM (model: 2100), Japan operating at 200 kV. Vibrational spectroscopy technique of Fourier transform infrared (FTIR) spectroscopy analysis has been carried out to investigate the role of clay concentration on the nature of polymer–ion interaction. The FTIR spectrum was recorded in the mid-frequency range (400–4000 cm^{-1}) at a scan rate of 32 with a wave number resolution of 4 cm^{-1} using Thermo Nicolet Spectrophotometer (Model: NEXUS–870). Electrical conductivity measurement on the composite films has been performed using a computer-controlled impedance analyzer (HIOKI LCR Hi-Tester Model: 3532, Japan) in the frequency range of 10 Hz to 1 MHz. The samples were placed in a symmetric cell configuration; SS|PNCE|SS (SS stands for stainless steel blocking electrodes) with an a.c. input signal of ~60 mV applied across the cell while carrying out impedance measurements on each of the PNC films having varying clay concentration. The glass-transition temperature has been measured by computer-controlled dynamic mechanical analyzer (TAInstruments, Lukens Drive, New castle, Delaware). The measurements were taken in tension mode in the appropriate temperature range (30–125 °C) at a heating rate of 2 °C min^{-1} and 1-Hz frequency.

Results

X-ray diffraction and TEM analysis

In order to obtain convincing evidence for intercalation/exfoliation of polymer salt complex into the nanometric clay channels, we have carried out a systematic analysis of the changes in the organomodified clay peak profile of PNC films. Figure 2 shows the representative HR-XRD pattern of pure clay, at lower (~2 wt%) and at higher organoclay concentration (15 wt%)-based polymer nanocomposite films. The feasibility of cation coordinated polymer chain intercalation/exfoliation into nanometric clay galleries has been investigated with reference to basic crystal structure of the organoclay (DMMT). In the present studies, sodium montmorillonite clay having monoclinic crystal structure [19] has been used where crystal axes "a" and "b" are continuous such that they have layered stack along "c" direction [20]. A schematic presentation of the layers and changes occurring in it on modification as well as intercalation is shown in Fig. 3a–c. The layers composed of edge shared octahedral sheet of aluminum hydroxide fanked by a tetrahedral silicate layers on either side. Experimental XRD pattern shows drastic changes in the d_{001} peak profile of the clay observed at 2θ–5.8° (Fig. 2a). X-ray diffractogram of PNC film with low clay concentration (2 wt%) exhibits typical features of

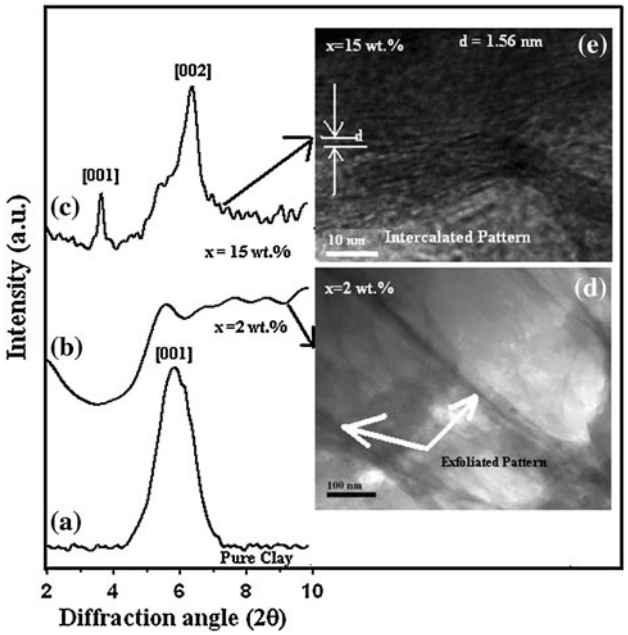

Fig. 2 Representative pattern of X-ray diffraction pattern of **a** $x = 0$ **b** $x = 2$ **c** $x = 15$, and TEM picture of **d** $x = 2$ **e** $x = 15$ wt% based on $(PAN)_8LiPF_6 + x$wt% DMMT

exfoliation (Fig. 2b). On the other hand, Fig. 2c depicts marked changes in the d_{001} peak pattern of clay observed in terms of peak shift toward lower angle side, increase in d-spacing and reinforced peak intensity for 15 wt% clay-loaded PNC. These changes suggest clear evidence for enhancement in the clay gallery width (W_{cg}) in the PNC films when compared with organoclay XRD data [7, 21]. These results provide clear indication of intercalation of polymer salt complex into the nanometric channels of organoclay as per the scheme suggested in the Fig. 3a–c. The possibility of exfoliation at lower and intercalation at higher clay loading has further been observed and corroborated by transmission electron microscopy (TEM) results (Fig. 2d–e) [22, 23]. A confirmation of nanocomposite formation with this approach is expected to maintain an effective separation between cation coordinated polymer chains and anion of the salt. This, in turn, should minimize the ion pairing/concentration polarization effect in the PNC. To confirm this, we have systematically analyzed the possibility and strength of interaction among composite components (i.e., polymer–ion–clay) using FTIR spectroscopy as a tool. The results are described as follows.

Fourier transform infrared (FTIR) analysis

Fourier transform infrared (FTIR) spectroscopy has been used to probe the possibility of interaction among the composite components at the microscopic level. Figure 4 shows the FTIR spectrum of PNC films based on $(PAN)_8$ $LiPF_6 + x$wt% DMMT with different organoclay concentrations ($x = 0$, 2, 7.5, 10, and 20) in the wavenumber region (400–3200 cm^{-1}). The characteristic absorption peak observed in the spectral pattern at the wavenumbers ~665, ~847, ~1071, ~1251, ~1653, ~2245, and 2940 cm^{-1} are attributed to $\delta(CH_2)$, $\nu(PF_6^-)$, bend(CH_2), w(CH_2), ν(C=O), $\nu(C\equiv N)$ and $\nu_a(CH_2)$, respectively [24–26]. The detailed assignment of the experimentally observed FTIR bands and effect of clay on changes in their

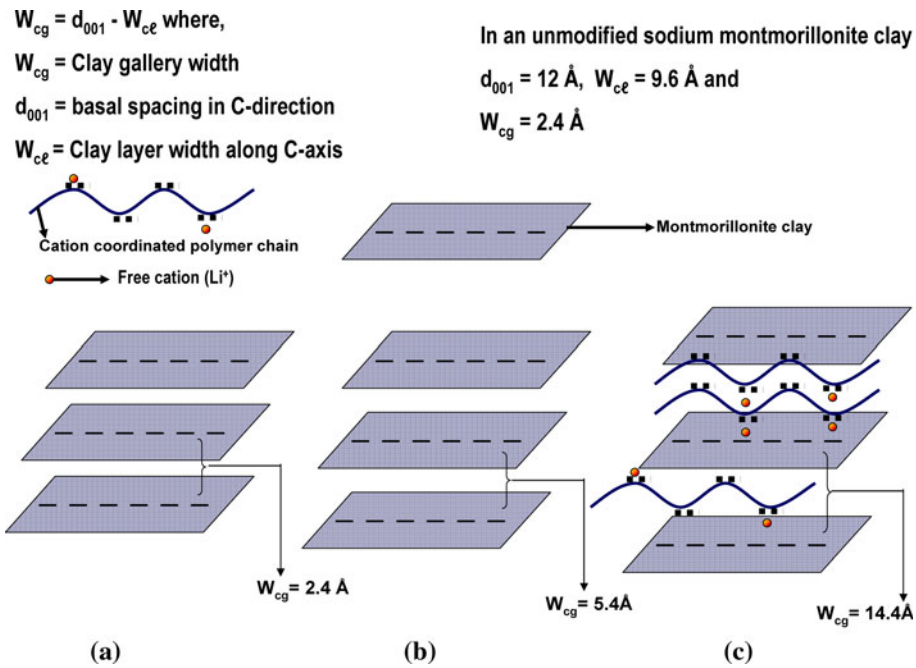

Fig. 3 Schematic representation of **a** NaMMT clay layers **b** changes occurring in it on modification **c** intercalation of cation coordinated polymer into the nanometric clay galleries of organoclay

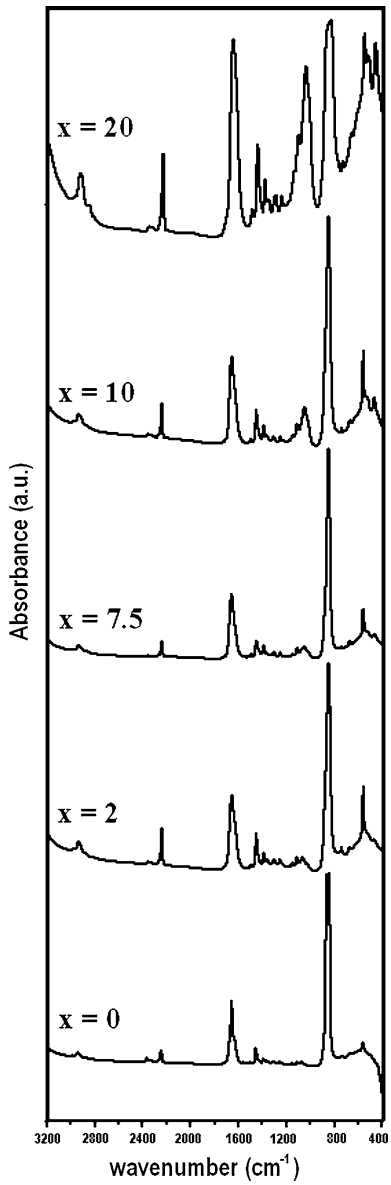

Fig. 4 FTIR spectrum of polymer nanocomposite based on $(PAN)_8$ $LiPF_6$ + *x*wt% DMMT clay

position with increasing clay concentration are recorded in the Table 1 A comparison of the band position clearly suggests that FTIR bands attributed to both the anions and the polymer chain groups undergo changes with varying concentration of organoclay in the composite phase. This is specifically pronounced in the case of PF_6^- band observed at wave numbers 847 cm^{-1} and PAN bands observed at wave numbers ~1071, 1360, 2245, and ~2940 cm^{-1}. These observations provide preliminary indication of an active role of organophilic clay (DMMT) in the polymer–ion, polymer–clay, ion–ion, and ion–clay interaction in polymer nanocomposite films. However, it requires a rigorous analysis before arising at any conclusion. A detailed analysis on the possibility of clay-induced interaction as evidenced in experimental result is presented briefly as follows.

Polymer–ion interaction

The characteristic absorption peak of host polymer (PAN) attributed to stretching of methylene (CH_2) group, nitrile group (–C≡N̈) and deformation mode (scissoring, wagging and twisting) of the methylene group of the polymer backbone has been observed to exhibit shift in band position (Table 1) on complexation with salt as well as addition of the organomodified clay into the cation coordinated polymer matrix. Table 1 indicates that the solvent swollen polymer band occurring at 1670 cm^{-1} undergoes on downward shift to 1635 cm^{-1} on complexation with salt. This lowering in band position suggests cation coordination at the electron-rich site of the solvent swollen polymer backbone. A similar observation of downward shift of the $\nu_s(CH_2)$ band of PAN from 2876 to 2872 cm^{-1} supports the possibility of change in chemical environment (attachment of additional groups) of the polymer host (PAN) backbone. These results provide strong evidence of polymer–ion interaction on addition of $LiPF_6$ in solvent swollen PAN. No evidence of salt interaction with solvent (DMF) skeletal groups (i.e., CH_3, C–CH_3, and C–N) could be observed in the FTIR spectrum. So, the possibility of ion–solvent interaction is ruled out. Further, the presence of a shoulder at 2270 cm^{-1} (near the C≡N̈) mode of PAN on salt addition (shown in Fig. 5) provides a clear evidence for interaction of ions of the salt with C≡N̈ site of the PAN backbone [27]. Strong electron donicity of C≡N̈ favors Li^+ coordination. These observations indicated beyond doubt that polymer ion interaction occurs with –C≡N̈ as the active site for Li^+ coordination. According to previous reports [28], the absorbance in the wavenumber region 2220–2300 cm^{-1} occurs due to two contributions; (a) uncoordinated –C≡N̈ at 2235–2255 cm^{-1} (b) cation coordinated –C≡N̈ at 2255–2280 cm^{-1}. Our observation appears to be consistent and convincing.

Ion–ion and ion–clay interaction

The typical vibrational modes of PF_6^- anion have been observed at 559 and 847 cm^{-1}. They are attributed to the deformation and stretching modes of PF_6^-, respectively. The $\nu_3(PF_6^-)$ band for polymer salt (PS) complex appearing at 847 cm^{-1} exhibits significant asymmetry as shown in the Fig. 6a. This asymmetric profile keeps on changing with change in the clay concentration in the composite phase (Fig. 6a–d). This asymmetry in the anion stretching vibrational mode is an outcome of the

Table 1 FTIR band assignment of polymer nanocomposite films based on $(PAN)_8LiPF_6$ + *x*wt% DMMT clay

PAN	PAN IN DMF	$(PAN)_8LiPF_6$ + *x*wt% NaMMT (organomodified clay)								Band assignment	
		$x = 0$	$x = 1$	$x = 2$	$x = 5$	$x = 7.5$	$x = 10$	$x = 15$	$x = 20$	Assigned mode	Source
–	–	–	–	–	466	467	465	465	466	def(SiO)	Clay
–	–	559	559	559	559	559	559	559	558	def(F–P–F')	Salt
666	665	669	669	669	669	671	668	668	669	def(CH_2)	PAN
773	773	741	741	741	741	740	741	741	741	rock(CH_2)	PAN
–	–	847	846	848	847	849	850	842	839	$\nu_a(F_2P)$	Salt
1075	1071	1071	1067	1065	1053	1057	1051	1050	1050	bend$(CH_2)^{\alpha}$	PAN
–	–	–	1111	1111	1111	1110	1111	1112	1112	ν(SiO)	Clay
1152	1151	1151	1151	1151	1151	1151	1149	1153	1153	twist(CH_2)	PAN
1252	1251	1251	1253	1253	1253	1253	1253	1252	1252	twist(CH_2)	PAN
1315	1313	1304	1304	1304	1305	1305	1305	1306	1304	twist(CH_2)	PAN
1362	1359	1360	1362	1363	1363	1365	1362	1363	1363	wag(CH_2)	PAN
–	–	–	1392	1392	1392	1391	1392	1391	1391	wag(CH_2)	PAN
1454	1455	1455	1455	1455	1455	1451	1455	1455	1452	scis(CH_2)	PAN
–	1670	1635	1655	1655	1658	1659	1659	1655	1658	ν(C=O)	Solvent
2245	2243	2245	2243	2243	2243	2245	2243	2243	2245	ν(C=N)	PAN
2876	2867	2872	2874	2867	2872	2872	2872	2872	2872	$\nu_s(CH_2)$	PAN
2940	2938	2940	2941	2941	2941	2941	2940	2940	2939	$\nu_a(CH_2)$	PAN

def deformation, *rock* rocking, ν_a asymmetric stretching, *bend* bending, ν_s symmetric stretching, *twist* twisting, *wag* wagging, *scis* scissoring

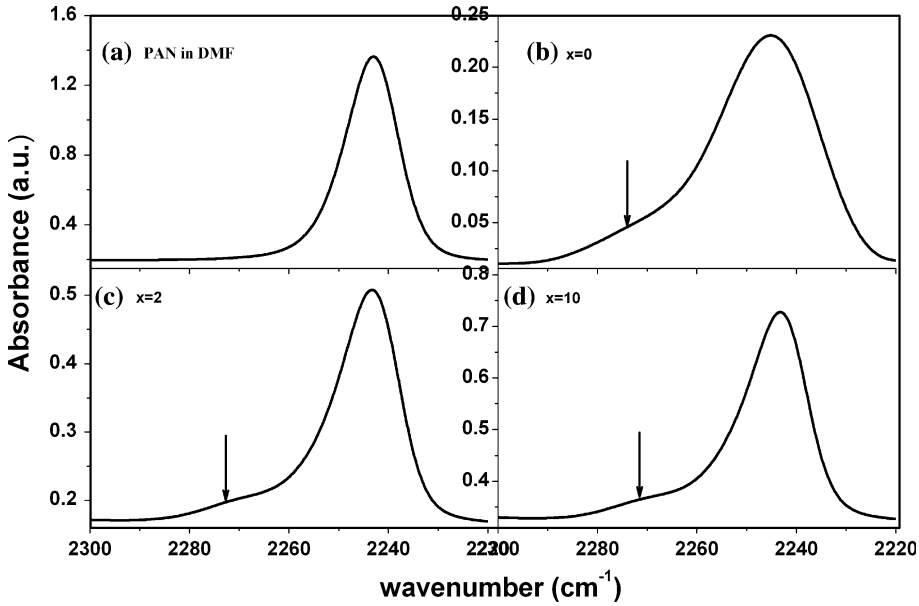

Fig. 5 The spectral band pattern of (–C≡N) in stretching mode of $(PAN)_8LiPF_6$ + *x*wt% DMMT clay composite

degeneracy arising out of more than one contribution possibly due to the presence of free anion (uncoordinated PF_6^-) and ion pairs (cation coordinated PF_6^-). In order to be sure for this possibility the $\nu_3(PF_6^-)$ band ($\sim$847 cm^{-1}) has been deconvoluted using Voigt profile with a commercial software peak fit. The deconvoluted pattern composed of two distinct contributions appearing at 843 and 862 cm^{-1} as shown in Fig. 6. The peak appearing at 843 cm^{-1} has been attributed to spectroscopically free anions and peak appearing at 862 cm^{-1} has been attributed to presence of ion pairs [29] in the solid polymer clay matrix. The presence of two distinct degenerate FTIR band in the experimental spectrum of $\nu_3(PF_6^-)$ provides an unambiguous evidences of strong ion–ion interaction in the PS and PNC films. The fraction of free anion and ion pair has been estimated quantitatively using the deconvoluted spectrum profile of $\nu_3(PF_6^-)$ of vibrational mode using the Eqs. 1a and 1b as given below.

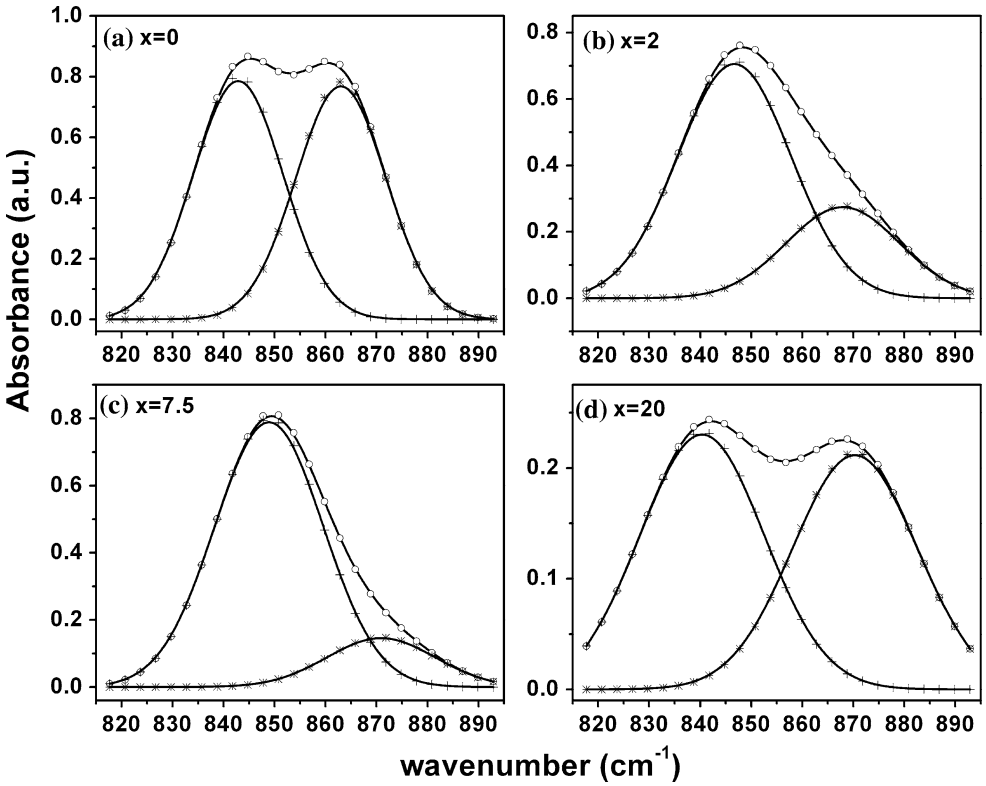

Fig. 6 Deconvolution pattern of $v_3(PF_6^-)$ in $(PAN)_8LiPF_6$ + *x*wt% DMMT clay composite

Table 2 Peak position of free anion and deconvoluted free anion peak of polymer nanocomposite films based on $(PAN)_8LiPF_6$ + *x*wt% DMMT clay

wt% clay conc.	Anion peak position (cm^{-1})	Deconvoluted anion peak data				Correlation coefficient (r^2)
		Free anion peak		Ion pair peak		
		Position (cm^{-1})	Area (%)	Position (cm^{-1})	Area (%)	
0	847	842	51	863	49	0.998
1	846	845	68	869	32	0.997
2	848	847	74	873	26	0.999
5	847	845	66	870	34	0.999
7.5	849	849	84	877	16	0.999
10	850	848	74	876	26	0.999
15	842	839	54	875	46	0.999
20	839	837	52	875	48	0.999

$$\text{Fraction of free anion} = \left(\frac{\text{Area of free anion peak}}{\text{Total peak area}}\right) \quad (1a)$$

and

$$\text{Fraction of ion pair} = \left(\frac{\text{Area of ion pair peak}}{\text{Total peak area}}\right) \quad (1b)$$

Figure 6b–d clearly depicts changing profile of deconvoluted pattern with a change in the clay loading in the PNC. It appears that even at a very low clay concentration (1–2 wt%), the fraction of free anion and hence free cation available in the PNC matrix appears to be more when the data is compared with that of pure polymer salt (PS) complex. Figure 6 provides a clear picture of enhancement in the available free charge carrier (Li^+ ions) on immediate addition of clay (2 wt%) into the polymer salt complex matrix. The fraction of free anion and hence fraction of free cations for various clay concentration in the PNC is shown in the Table 2. A comparison indicates relatively higher fraction of free charge carriers at 2 and 7.5 wt% clay concentration. Beyond this, the free anion fraction gets reduced; however, the available free charge carrier is still more in the composite film in comparison to that of the PS.

These results clearly suggest convincing evidence for clay assisted ion dissociation effect in the polymer nanocomposite films. This feasibility due to stronger clay–ion interaction seems logical in view of the dipolar characteristics of montmorillonite clay.

The variation in free anion fraction with clay concentration (Table 2) is expected to have a direct impact on electrical transport. Such a correlation would be discussed subsequently in this article.

Polymer–ion–clay interaction

The effect of clay addition in the cation coordinated polymer matrix has resulted in substantial changes in the FTIR spectrum profile of polymer backbone (PAN). This is indicated by clay concentration-dependent spectral changes recorded in the wavenumber regions ~500–600, 1000–1100, 1330–1410, 2200–2300, and 2900–3000 cm^{-1} attributed to bending mode of PF_6^- as well as deformation mode of (Al–O–Si), bending of CH_2, wagging mode of CH_2, (–C≡N̈) stretching and CH_2 asymmetric stretching mode respectively. The changes have been noticed in terms of shifting in band position, appearance of additional band/shoulder and marked asymmetry in the band profile with variation in the clay loading in the PNC matrix. These results, which may be an outcome of the interaction of clay with polymer and ion component of the PNC matrix, are described systematically as follows.

The spectral band pattern in the wavenumber region 500–600 cm^{-1} has been deconvoluted using the Voigt amp profile with peak fit software. The asymmetry in the band profile shows clear presence of an additional peak attributed to clay in this region. Two distinct contributions appearing at 533 and 559 cm^{-1} are shown in the Fig. 7a for PS. The band appearing at lower wavenumber (533 cm^{-1}) is attributed to free anion and wavenumber appearing at higher wavenumber (559 cm^{-1}) is attributed to ion pair contribution. Further, it has been noticed in the Fig. 7 that at lower clay loading in PS matrix, the intensity of the band at 533 cm^{-1} gets strengthened whereas that of the band appearing at 559 cm^{-1} remains unaffected. As the clay loading becomes high ($x \geq 10$ wt%) an additional peak appears at 520 cm^{-1}. This has been identified as the clay peak attributed to the deformation mode of Al–O–Si. Appearance of δ(Al–O–Si) mode at $x \geq 10$ wt% of clay shows clear evidence of interaction of clay with polymer salt matrix. It should be mentioned here that intercalated form of composite matrix exists at higher clay loading as evidenced from XRD results (Fig. 2).

Figure 8 shows the spectral pattern of bending mode of CH_2 band of the host polymer in the region 1,000–1,100 cm^{-1}. The peak appearing at 1075 cm^{-1} attributed to bending mode of CH_2 changes its profile on cation coordination with polymer backbone. A systematic change in the profile occurs on clay loading with downward shift as recorded in the Table 1. In solvent swollen

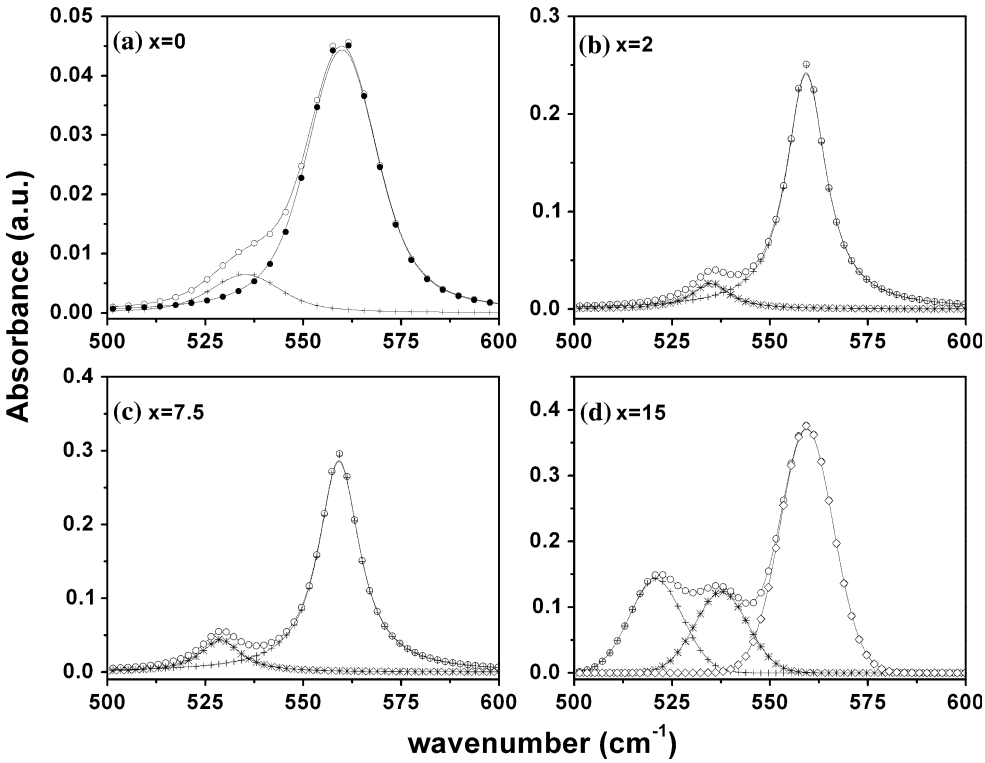

Fig. 7 The evidences of appearing of clay peak in $\nu_4(PF_6^-)$ in $(PAN)_8LiPF_6$ + *x*wt% DMMT clay composites

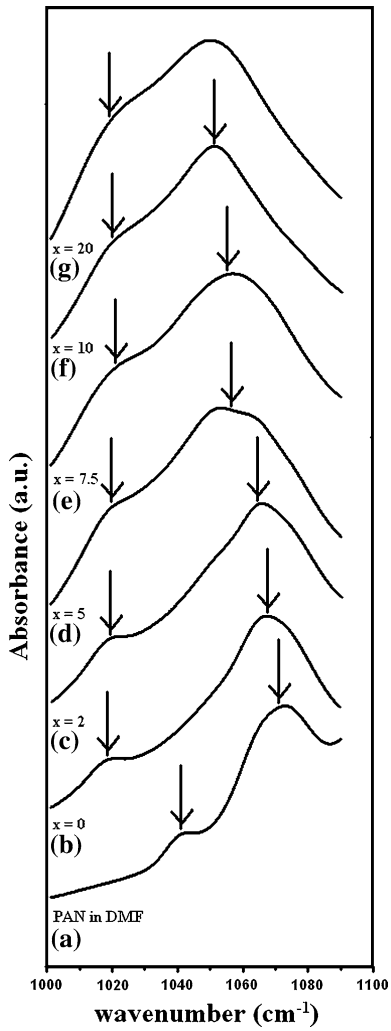

Fig. 8 The spectral band pattern of twisting mode CH_2 in PNC film based on $(PAN)_8LiPF_6$ + *x*wt% DMMT clay

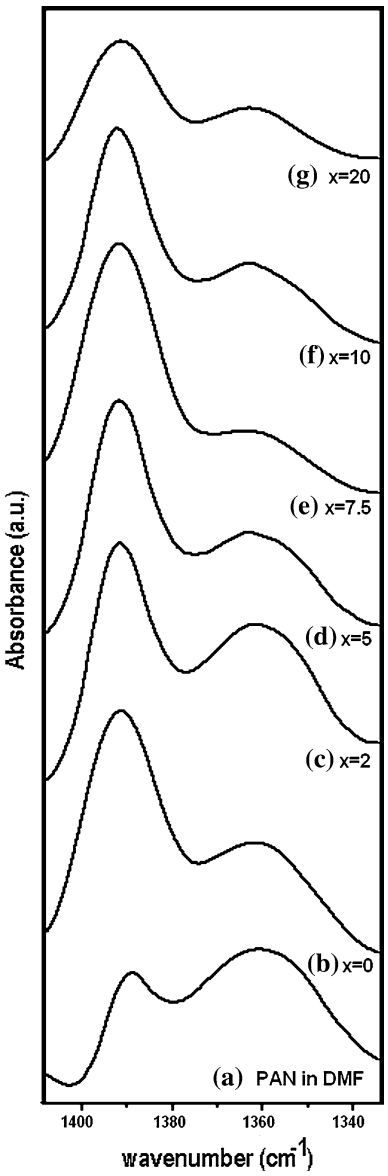

Fig. 9 Changes in band profile of wagging mode of CH_2 in $(PAN)_8LiPF_6$ + *x*wt% DMMT clay-based films

polymer (PAN), the presence of a shoulder at $\sim$1045 cm^{-1} has been noticed (Fig. 8a). On polymer salt complexation, the shoulder becomes diffused with a downward shift at $\sim$1028 and 1075 cm^{-1} peak also shifted toward lower wavenumber side. It may be due to polymer–ion interaction in the PS film. On adding the organomodified clay in the PS matrix, the shoulder at 1045 cm^{-1} gets diffused further even at low clay loading ($\sim$2 wt%) and vanishes at higher clay loadings. On the other hand, the peak at 1075 cm^{-1} undergoes significant broadening and shows downward shift on higher clay loadings (Fig. 8). These evidences suggest strong possibility of polymer–ion–clay interaction in the PNC phase. This possibility is further corroborated by the changes in the intensity ratio of the CH_2 breathing (wagging) vibrational mode of PAN skeleton appearing in the wavenumber region $\sim$1330–1410 cm^{-1}. The two distinct contributions appearing at $\sim$1362 and $\sim$1390 cm^{-1} undergo relative change intensity profile with varying clay concentration (Fig. 9). The wagging mode of CH_2 appearing initially as a well resolved peak at 1362 cm^{-1} becomes a shoulder for clay concentration $x \geq 10$ wt%. An analogous effect can be seen in terms of clay-induced changes in the spectrum profile of $\nu_a(CH_2)$ band attributed to host polymer skeleton vibrational mode. This is depicted in the Fig. 10. The spectrum clearly shows noticeable change indicated by peak broadening and appearance of shoulder that changes its profile in the spectrum with clay concentration. The weak shoulder observed in the solvent swollen polymer host matrix appears to vanish on immediate addition of salt and it reappears with substantial peak broadening at $x = 2$ wt% clay concentration. Further clay addition reinforces the effect. These results observed in the

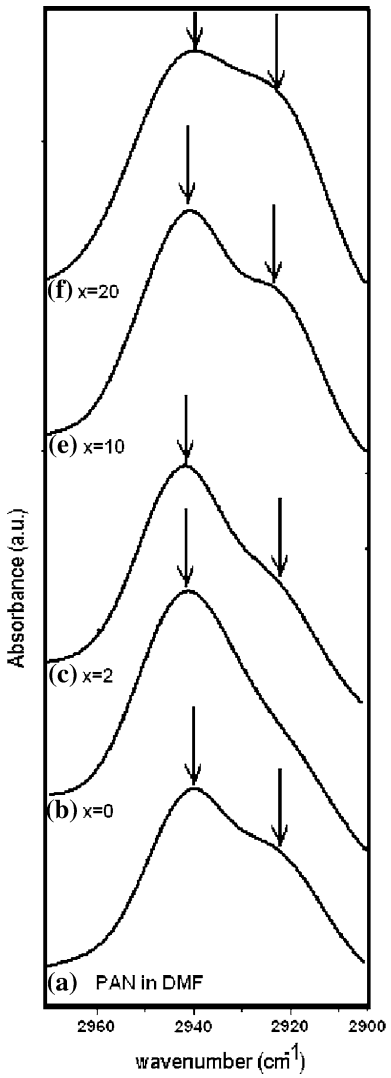

Fig. 10 Changes in band profile of asymmetric stretching mode of CH_2 in $(PAN)_8LiPF_6$ + *x*wt% DMMT clay film

FTIR spectrum provide strong and convincing evidence for interaction among the composite components of the PNC films, i.e., polymer–ion–clay interaction. Such an interaction causes substantial impact on ion association/dissociation process in the heterogeneous PNC matrix. Clay-induced ion dissociation would release free mobile charges and assist in enhancement in the ion transport properties of the PNC films. This is analyzed as follows.

Role of clay concentration on ion dynamics and mobile charge carrier concentration

The electrical conductivity in PNC films has been analyzed and evaluated using complex impedance spectroscopy technique. The representative complex impedance spectrum (CIS) pattern of PNC films ($x = 0$ and $x = 7.5$ wt%) at room temperature is shown in Fig. 11. It shows a typical response, comprising a semicircular arc in the high-frequency region followed by a steeply rising spike in the low-frequency region. The intercept of the semicircular arc with the spike on real axis gives an estimate of the sample bulk resistance (R_b). A non-linear least square fitting of the impedance response of PS films agrees well with an electrical equivalent circuit model comprising a parallel combination of resistance (R) and constant phase element (CPE) in series combination with another CPE. The presence of constant phase element in a sample response is a testimony of its multiphase characteristics comprising a microstructure having both crystalline and amorphous phases. The impedance of CPE is normally represented as $Z_{CPE} = \frac{1}{Q_0(i\omega)^n}$, where $i = \sqrt{-1}$, Q_0 and "n" are fitting parameter such that it may behave as an electrical analogue of resistance, Warburg impedance capacitance and inductance for different values of $n = 0$, 0.5, 1, and -1,

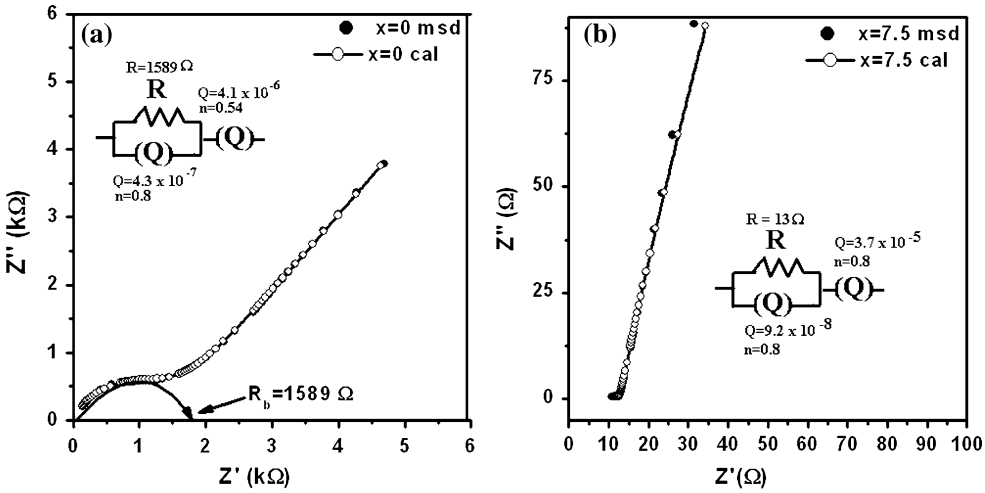

Fig. 11 The representative CIS pattern of polymer nanocomposite ($x = 0$ and $x = 7.5$ wt%) films at room temperature

respectively. The electrical conductivity has been estimated with the bulk resistance (R_b) obtained from complex impedance result, using the formula $\sigma_{dc} = \frac{1}{R_b}\frac{\ell}{A}$. This process has been followed for all the PNC samples and their conductivity (room temperature and at 100 °C) has been observed as a function of clay concentration. Larger the conductivity higher is the availability of the mobile charges.

Figure 12 shows the representative pattern of mechanical loss peak (tanδ vs. temperature) of PNC for $x = 0$, 2, and 15 wt% observed in the DMA result. The glass-transition temperature (T_g) has been estimated from loss peak of dynamic mechanical analysis results. Peak asymmetry prompted us to use Voigt profile fitting of the temperature evolution of mechanical loss pattern. It gave two distinct contributions in the tanδ versus temperature profile. The deconvoluted mechanical loss peak occurring at lower temperature is attributed to the glass-transition temperature of the polymer salt (PS) complex, whereas the high-temperature loss peak may be related to the glass-transition temperature of PAN. The glass-transition temperature peaks in the DMA loss pattern basically refers to the structural phase transition from a rigid framework structure (plastic phase) to an elastomeric (rubbery) phase under thermomechanical stress. This estimate for T_g is therefore considered more reliable than that from DSC. Results indicate that a lowering in the glass-transition (T_g) temperature occurs at lower clay concentration when compared with respect to that of the PS. A relative lowering in the T_g at lower clay loading points toward enhancement in the flexibility of the polymer backbone. This in turn may be expected to increase polymer chain motion in the PNC phase. Since cation coordination occurs at electron-rich site (–C≡N̈) of the host polymer, any enhancement in the polymer chain motion would favours faster ion dynamics such an effect, therefore may cause substantial tailoring of electrical conductivity of the PNC films depending on the fraction of clay loading.

The electrical conductivity, estimated at room temperature for various clay concentrations is shown in Fig. 13a. A comparison suggests an immediate enhancement by ~26 times in the conductivity for ~2 wt% clay when compared with that of PS film. This may be attributed to the release of free charge carriers due to polymer–ion–clay interaction. Such an interaction causes significant ion dissociation due to an active role of clay in weakening the co-ordination bond between –C≡N̆–Li^+ ion. This feasibility seems logical and valid in view of the experimental evidences from FTIR analysis. Further, an increase in clay concentration modulates the electrical conductivity of the polymer nanocomposite films drastically. A maximum electrical conductivity ~3.7×10^{-3} S cm^{-1} (~110 times) has been observed for 7.5 wt% organoclay loading in the PNC at room temperature (Fig. 13a). This change may be related to the combined effect of polymer chain flexibility (lowering of glass transition temperature) as well as increase the number of free charge carrier at room temperature. Lower the glass-transition temperature, higher the polymer chain flexibility causing enhanced dynamics of cation coordinated polymer chain. This in consequence, would increase the rate of charge migration. Converse is true for an increase in glass-transition temperature. An excellent correlation of the

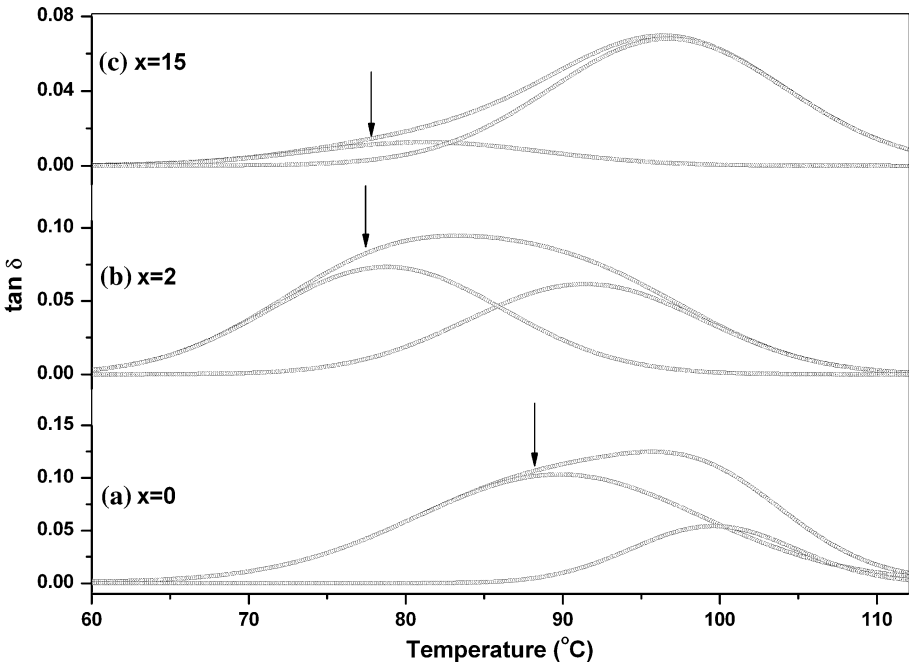

Fig. 12 The representative loss pattern (tanδ vs. temp in DMA) of PNC films based on $(PAN)_8LiPF_6$ + $x$wt% DMMT clay at $x = 0$, 2, 15 from DMA analysis

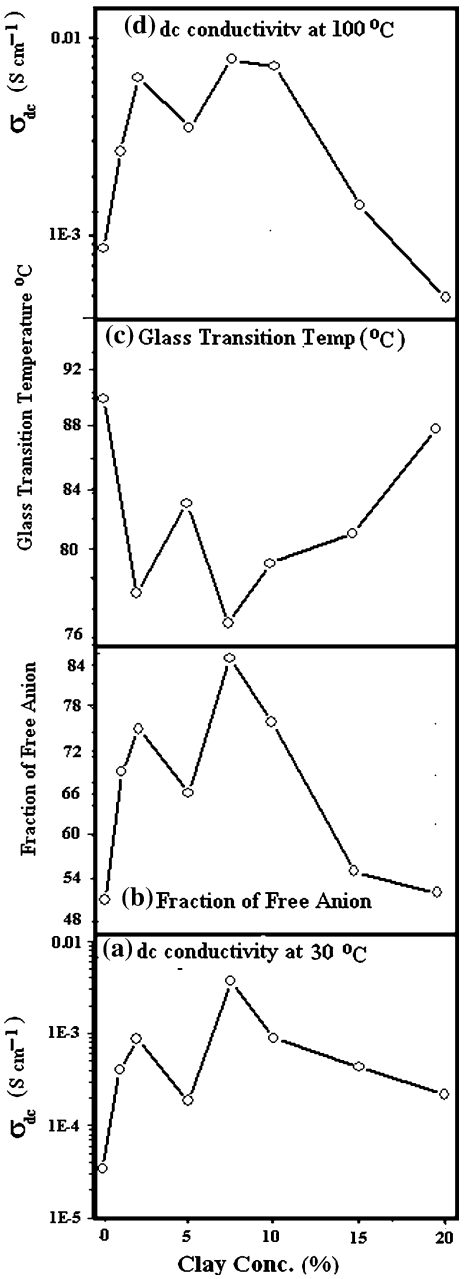

Fig. 13 The correlation spectrum of dc conductivity, fraction of free anion and glass-transition temperature of PNC films based on $(PAN)_8LiPF_6 + x$wt.% DMMT clay

minima in T_g and maxima in the fraction of free anion variation with the maxima in the σ_{dc} variation with organoclay concentration (Fig. 13a–d) appears convincing in support of our proposition. These types of variation of these physical parameters with organoclay concentration are reported in literature earlier also [30, 31]. The experimental result of electrical conductivity in polymer nanocomposite films depends strongly on the number of free mobile charge carrier in the sample matrix available for charge transport. It is estimated from the quantification of deconvoluted FTIR profile of $v_3(PF_6^-)$ band. The enhancement of free mobile charge carrier causes a substantial increase in electrical conductivity that appears to be consistent and logical in accordance with the relation;

$$\sigma_{dc(total)} = \sum_i q_i n_i \mu_i$$

where n_i is the fraction of free anion/cation, q_i is ionic charge, and μ_i is ionic mobility. Since q_i and μ_i are constant for a particular ionic system; the dc conductivity may be considered directly proportional to the number of free anion/and hence free cation fraction (n_i). As a consequence, conductivity would be higher at a clay concentration where value of n_i is higher, i.e., more number of free mobile charge carrier are available.

Discussion

An excellent correlation between free mobile charge concentration and dc conductivity variation w.r.t. organoclay concentration suggests an active role of clay in the release of charge carriers for mobility in the PNC matrix. Evidence of this possibility has been provided in the FTIR results in terms of polymer–ion–clay interaction. The bulky anion PF_6^- present in polymer nanocomposite films ($(PAN)_8$ $LiPF_6 + x$wt% DMMT) is highly sensitive to FTIR and Raman excitations with a probability of 15 (3N-6; $N = 7$) fundamental vibrational modes, [29, 32, 33] in its free (uncoordinated) state, arising out of its octahedral (O_h) symmetry. The 15 vibration modes of free PF_6^- anion can be represented as

$$\Gamma = a_{1g} + e_g + 2t_{1u} + t_{2g} + t_{2u}$$

Of these modes, $v_1(a_{1g})$, $v_2(e_g)$, and $v_5(t_{2g})$ are Raman active having degeneracy 1, 2, and 3, respectively. On the other hand, $v_3(t_{1u})$ and $v_4(t_{1u})$ modes are IR active with degeneracy three each, whereas the triply degenerate $v_6(t_{2u})$ mode is inactive in both IR as well as the Raman spectrum.

Any possible co-ordination of PF_6^- group with counter ions usually results in lowering of the PF_6^- symmetry from O_h to $C_{4v}/C_{2v}/C_{3v}$ depending on the nature of the cation coordination (monodentate/bidentate/tridentate) with PF_6^- group. Structural symmetry of hexafluorophosphate anions (PF_6^-) in its free state and state of interaction with Li^+ ion are shown schematically in the Fig. 14a–d. The distinct possibilities of Li^+ coordination with PF_6^- seem consistent with its maximum coordination number ~ 5. The weaker ion–ion interaction is represented by Fig. 13b. As the number of F-atom bonded to Li^+ increases the strength of ion–ion interaction become stronger.

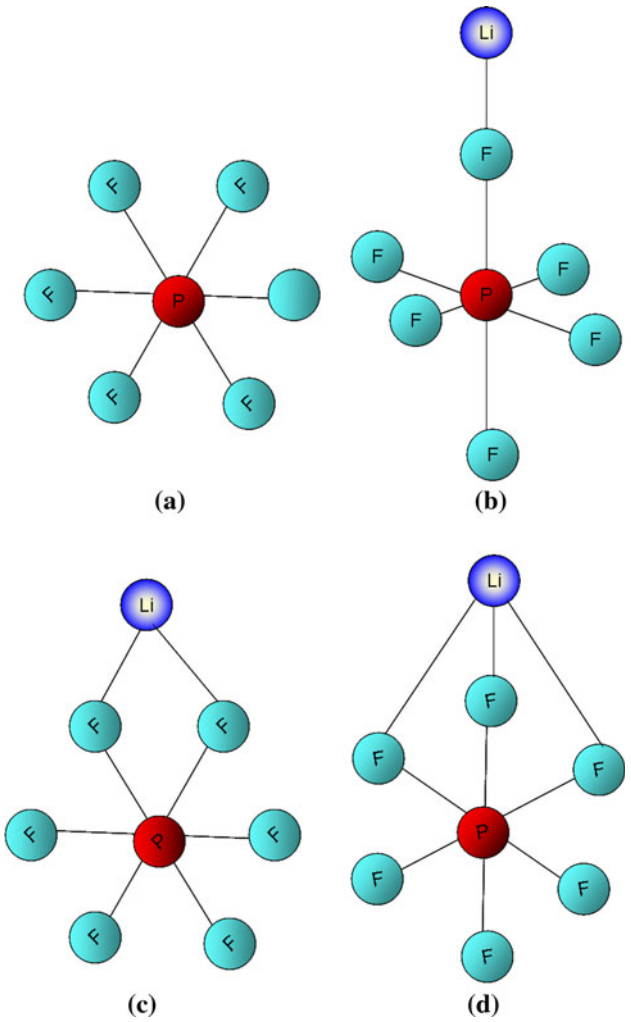

Fig. 14 Structural symmetry of hexafluorophosphate anions (PF_6^-) during free state and state of interaction **a** free anion, b monodentate, **c** bidentate, **d** tridentate

Scheme

A number of models have been proposed to explain the filler/clay-dependent changes in electrical properties of the composite phase. The central idea of all such models is based on a concepts including; (i) Lewis acid–base interaction between polymer–ions–fillers [34, 35], (ii) adsorption of polymer onto the filler surface and (iii) van der Waals interaction between filler particles [36]. The gist of most of the models lies in accepting the role of the fillers as a supporting matrix in the composite phase [37]. The role of organophilic clay in an intercalated composite matrix and its impact on variation of electrical conductivity in the composite phase has not yet been explored. The experimental evidences from FTIR spectroscopy, conductivity, and polymer glass transition dependence on clay loading has prompted us to analyze and propose a model to explain the charge transport mechanism. It is discussed below.

In the case of pristine PS matrix, Li^+ cation may expected to have a coordination number $\sim$4, 5, and 6 [38–40] depending upon the chemical environment around free lithium cations. This suggest that Li^+ cation may get coordinated at the most with 4, 5, or 6 electron-rich nitrogen (–C≡N̈) sites of the polymer host matrix due to polymer–ion–clay interaction evidenced in FTIR results. In this case, the bulky anion (PF_6^-) is expected to remain hanged somewhere in the polymer backbone as an uncoordinated free anion as per the scheme proposed in the Fig. 15 (stage 1). Such a possibility has already been evidenced in the FTIR results (Fig. 6).

Stage 1 of the model shown in the Fig. 15 depicts a scheme for possible polymer-cation coordination which can be of two types: (i) direct coordination of cations with electron-rich site (–C≡N̈) of the polymer chains and/or (ii) coordination of cations to polymer chain bridged by anions. The former possibility seems more feasible during the polymer salt complexation. Initially, the presence of negative charge at the surface of nanometric clay galleries favors easier entry of cation coordinated polymer chains into it. Such a feasibility is thermodynamically viable ($\Delta G = -Ve$) as well as favored by coulombic interaction between the cation coordinated polymer and clay surface having $-$ve charges on it. This is shown in stage 2 of Fig. 15. In view of an evident feasibility of ion–clay interaction, observed in the FTIR results on ion–ion and ion–clay interaction, the dipolar clay platelets may be expected to interact strongly with the cation coordinated (–C≡N̈) group in the polymer backbone. In fact, it seems reasonable in view of the Lewis base properties of the –C≡N̈ group. At lower clay loading in the PNC, the number of channels available in the clay (component 1) is far less than the quantity of cation coordinated polymer chains (component 2) seeking entry. The coulombic interaction between the two components of the composite creates an imbalance resulting into the rupture of clay platelets. As a consequence exfoliation is the natural possibility. This is depicted in the stage 2 (2A). As the clay concentration increases, the number of available clay galleries becomes large with the possibility to accommodate larger fraction of cation coordinated polymer chains. As a result, intercalation occurs as evidenced in XRD and TEM results (Fig. 2). This possibility has been represented schematically in the stage 2 (2B).

The next step in this model is to explain the clay concentration-dependent tailoring in d.c. conductivity. An enhancement in the conductivity of the composite phase depends on a number of factors such as (i) polymer glass transition and local chain motion, (ii) electrical properties of each component in the PNC and their effective strength in the composite structure, (iii) interaction among components in the nanocomposite matrix, (iv) number of

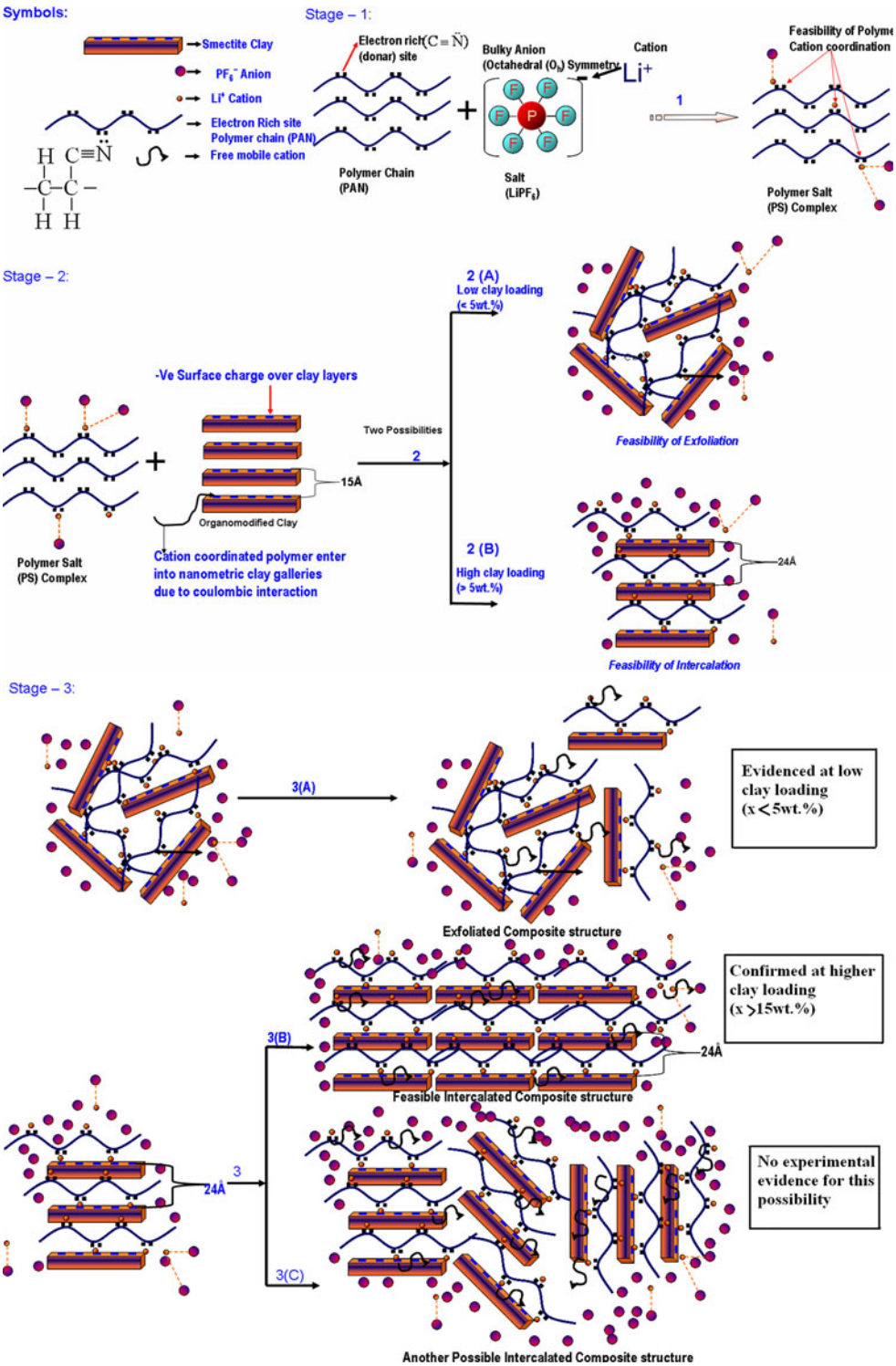

Fig. 15 Scheme based on ion conduction mechanism, *step 1*: cation coordination with polymer backbone side, *step 2*: possibility of interaction of cation coordinated polymer with clay tactoids, *step 3*: release of free charge carriers (cations) from the coordinated polymer chains on addition of clay in the PNC films

available free charge carrier for mobility in the heterogeneous nanocomposite phase, and (v) distribution of the composite components, etc. A comparison of d.c. conductivity, in the present investigation, indicates a clear enhancement by ~26 times at room temperature and ~8 times at 100 °C at a clay loading of 2 wt% in the PNC relative to PS. This enhancement may be related to the direct interaction of organophilic dipolar clay platelets with the cation coordinated polymer chain due to Lewis acid–base-type interaction. This possibility seems logical

because –C≡N̈–Li^+ site in the polymer chain behaves as a Lewis base, whereas the organophilic clay acts as Lewis acid. Evidences of such an interaction in the PNC phase has been noticed in terms of polymer–clay and ion–clay interaction in the FTIR results of Figs. 5–10, respectively. As a consequence the coordinated cations are released and become available as a free mobile charge carrier. An enhancement in the fraction of free anions at 2 wt% clay loading noted in the FTIR results (Fig. 6), provides evidence of clay-assisted conductivity enhancement. This enhancement is further supported by a lowering in the T_g at 2 wt% (Fig. 13) causing flexibility in the polymer backbone/enhancement in the local chain motion of the polymer backbone. The net conductivity enhancement, although relatively lower at 2 wt%, is the result of direct interaction of clay platelets with the Li^+ coordinated polymer that seems logical in the exfoliated PNC. As the clay concentration increases, a redistribution of the clay occurs in the composite phase whereby a rearrangement from exfoliated to intercalated nanocomposite structure is the likely possibility. Feasibility of such a structural change and modulation in the distribution of clay platelets may possibly weaken the interaction among composite components. So, the availability of free mobile charge carrier decreases (Table 2) with further rise in clay concentration ($x > 5$ wt%). Intercalation of the cation coordinated polymer chains into the nanometric clay galleries has been confirmed in the experimental results (Fig. 2) with significant enhancement in the width of clay galleries displayed schematically in Fig. 3. These evidences suggest that entry of cationic charge (Li^+) along with polymer chain into the organophilic clay galleries at higher clay loading ($\sim$7.5 wt%) facilitate an effective separation of cation (Li^+) from the counter ion (PF_6^-). The outcome is minimization of ion pairing/concentration polarization leading to maximization of charge transport in the PNC film. This hypothesis is strongly supported by a very large enhancement in the room temperature conductivity (by $\sim$110 times) at 7.5 wt% clay concentration in the PNC. The FTIR results of Figs. 5–10) and the excellent correlation of σ_{dc}, T_g, and FFA observed in Fig. 13 are convincing testimony for the proposed idea and seem consistent with the models presented in the stage 3A and 3B of Fig. 15.

The final drop in conductivity at elevated clay concentration may be related to the random/disordered distribution of clay particulates in the composite phase as per the scheme proposed in stage 3C. Although no direct evidence for this possibility could be noticed in experimental results, an enhancement in T_g (Fig. 13) at higher clay concentration ($x \geq 10$ wt%) supports lowering of polymer chain dynamics.

Conclusions

We report experimental results on ion-conducting polymer–clay nanocomposite films in exfoliated and intercalated phases spread over a different loading fractions of the clay in the PNC. The possibility of exfoliation/intercalation is confirmed in XRD/TEM results. FTIR results indicated clear evidence for polymer–ion, ion–ion, and polymer–ion–clay interaction. Evidences suggest that coordination of PF_6^- group with counter ions usually results in lowering of the PF_6^- symmetry from O_h to $C_{4v}/C_{2v}/C_{3v}$ depending upon the nature of cation coordination. DMA analysis gives two distinct contributions for glass-transition temperature of the host polymer in the tanδ versus temperature profile. Lower temperature shows the glass-transition temperature of polymer salt complex, whereas the higher temperature has been attributed to the glass-transition temperature of host polymer. An excellent correlation of the changes in glass-transition temperature with fraction of free charge carriers and σ_{dc} has been noticed in the present investigation. A mechanism for clay-induced charge transport in the PNC has been proposed to explain the observed changes on the basis of polymer–ion–clay interaction. Proposed mechanism appears to be consistent and convincing on in the light of experimental results.

Acknowledgments One of us (Achchhe Lal Sharma) gratefully acknowledges the financial support received from Council of Scientific and Industrial Research (CSIR), Govt. of India, New Delhi for carrying out research at the Department of Physics and Meteorology, Indian Institute of Technology (IIT) Kharagpur-721302, INDIA.

References

1. Reiter J, Krejza O, Sedlarikova M (2009) Sol Energy Mater Sol Cells 93:249
2. Rajendran S, Babu RS, Sivakumar P (2008) J Membr Sci 315:67
3. Bhide A, Hariharan K (2007) Eur Polym J 43:4253
4. Ballav N, Sardar PS, Ghosh S, Biswas M (2006) J Mater Sci 41:2959. doi:10.1007/s10853-006-6716-3
5. Zhou S, Fang S (2007) Eur Polym J 43:3695
6. Geiculescu OE, Yang J, Blau H, Walsh RB, Creager SE, Pennington WT, Desmarteau DD (2002) Solid State Ionics 148:173
7. Mohapatra SR, Thakur AK, Choudhary RNP (2009) J Power Sour 191:601
8. Wang Y, Ma X, Zhang Q, Tian N (2010) J Membr Sci 349:279
9. Osinska M, Walkowiak M, Zalewskab A, Jesionowski T (2009) J Membr Sci 326:582
10. Zhang J, Huang X, Fua J, Huang Y, Liu W, Tang X Mater Chem Phys. doi:10.1016/j.matchemphys.2010.02.016
11. Qiao H, Luan H, Zhou Z, Bi L, Yao W, Li J, Chen C (2008) J Mol Struct 885:89
12. Sun S, Lin Y, Jing X (1996) Solid State Ion 83:79
13. Basumallick I, Roy P, Chatterjee A, Bhattacharya A, Chatterjee S, Ghosh S (2006) J Power Sour 162:797
14. Kalpana D, Renganathan NG, Pitchumani S (2006) J Power Sour 157:621

15. Min HS, Kang DW, Lee DY, Kim DW (2002) J Polym Sci B 40:1496
16. Kumar GG, Munichandraiah N (2002) Electrochim Acta 47:1013
17. Utracki LA, Kamal MR (2002) Arab J Sci Eng 27:43
18. Sharma AL, Thakur AK (2009) Ionics. doi:10.1007/s11581-009-0394-5
19. Siri AG, Brocorens P, Siri D, Gardebien F, Bredas JL, Lazzaroni R (2003) Langmuir 19:8287
20. Aranda P, Hitzky ER (1992) Chem Mater 4:1395
21. Kim S, Park SJ (2007) Solid State Ionics 178:973
22. Ray SS, Okamoto M (2003) Prog Polym Sci 28:1539
23. Giannelis EP (1996) Adv Mater 8:29
24. Deepa M, Sharma N, Agnihotry SA, Chandra R (2002) J Mater Sci 37:1759. doi:10.1023/A:1014921101649
25. York SS, Boesch SE, Wheeler RA, Frech R (2002) Phys Chem Commun 5:99
26. Huang B, Wang Z, Li G, Huang H, Xue R, Chen L, Wang F (1996) Solid State Ionics 85:79
27. Yoon HK, Chung WS, Jo NJ (2004) Electrochim Acta 50:289
28. Yang YWC, Chen YT, Chen HC, Lin WC, Tsai CH (2009) Polymer 50:2856
29. Xuan X, Wang J, Wang H (2005) Electrochim Acta 50:4196
30. Dissanayake MAKL, Jayathilaka PARD, Bokalawala RSP, Albinsson I, Mellander BE (2003) J Power Sour 119–121:409
31. Mohapatra SR, Thakur AK, Choudhary RNP (2009) J Polym Sci B 47:60
32. Grondin J, Ducasse L, Bruneel JL, Servant L, Lassegues JC (2004) Solid State Ionics 166:441
33. Ducasse L, Dussauze M, Grondin J, Lassegues JC, Naudin C, Servant L (2003) Phys Chem Chem Phys 5:567
34. Jayathilaka PARD, Dissanayake MAKL, Albinsson I, Mellander BE (2002) Electrochim Acta 47:3257
35. Marcinek M, Bac A, Lipka P, Zalewska A, Zukowska G, Borkowska R, Wieczorek W (2000) J Phys Chem B 104: 11088
36. Yina X, Hong L, Liu Z (2005) J Eur Ceram Soc 25:3097
37. Ali Z, Le HH, Ilissch S, Radusch HJ (2009) J Mater Sci 44:6427. doi:10.1007/s10853-009-3892-y
38. Izatt RM, Bradshaw JS, Dalley NK (1881) Chem Rev 91:137
39. Enderby JE (1995) Chem Soc Rev 159:168
40. Wang Z, Huang B, Xue R, Huang X, Chen L (1999) Solid State Ion 121:141